Article

Bio-inspired porous ZnO nanomaterials from fungal polysaccharides: advanced materials with unprecedented low toxicity in-vitro for human cells

Chunping Xu, Rick Arancon, Manuel Ojeda, Antonio Angel Romero, Jose Luis Domingo, Mercedes M Gomez, Jordi Blanco, and Rafael Luque

ACS Sustainable Chem. Eng., **Just Accepted Manuscript** • DOI: 10.1021/acssuschemeng.5b00568 • Publication Date (Web): 14 Sep 2015

Bio-inspired porous ZnO nanomaterials from fungal polysaccharides: advanced materials with unprecedented low toxicity *in-vitro* for human cells

Chunping Xu[a], Manuel Ojeda[b], Rick A.D. Arancon[b], Antonio A. Romero[b], José Luis Domingo[c], Mercedes Gómez[c], Jordi Blanco[c], Rafael Luque[*b]

[a]*School of Food and Biological Engineering, Zhengzhou University of Light Industry, Dongfeng Road 5, Zhengzhou, Henan, 450002, P.R. China, e-mail: c.p.xu@zzuli.edu.cn*

[b]*Departamento de Química Orgánica, Universidad de Córdoba, Edificio Marie Curie (C-3), Ctra Nnal IV-A, Km 396, E14014, Córdoba (Spain), e-mail: q62alsor@uco.es*

[c]*Laboratory of Toxicology and Environmental Health, School of Medicine, IISPV, Universitat Rovira i Virgili, 43201 Reus, (Spain), e-mail: joseluis.domingo@urv.cat*

Abstract

Mechanochemically synthesized ZnO-polysaccharide nanohybrids prepared from fungal polysaccharides were proved to exhibit remarkable surface properties and structures for biomedical applications. The synthesized ZnO nanomaterials possessed an unprecedented low cytotoxicity against human cell lines A549 and SH-SY5Y (EC50: 50-100 μg mL^{-1}) as compared to commercial ZnO nanomaterials due to the stability and low release of Zn^{2+} and reduced interaction nanoparticle/cells due to the high biocompatibility of the nanohybrids.

Keywords: ZnO; mechanochemistry; cytotoxicity; bionanomaterials

Introduction

Nature serves as inspiration to scientists in innovation and the design of advanced materials able to serve the basis of the expected future demands in resource scarcity, water, energy and food. The miniaturisation and efficiency achieved by common entities in nature in the production of energy, biometabolites, photo-processing and resource maximisation has always been attractive to imitate based on fundamental and rational understanding.[1,2] The field of nanomaterials has experienced remarkable advances in recent years motivated by fascinating discoveries and progress brought by both unique and excelling properties of nanoentities conferred by their small sizes, high surface areas and energies as well as degenerated density of energy states. A number of advanced nanomaterials have been therefore designed for a large number of applications including biomedical devices, electronics, catalysis, information technologies, food packaging and preservation, personal care products, as well as environmental technologies.[3]

Generally speaking, most preparation protocols of advanced materials for various applications possess inherent shortcomings which include an excessive use of solvents, high temperatures and/or pressures, expensive reagents (e.g. noble metals) and hazardous chemicals and/or reaction conditions, sophisticated equipment and tedious workup protocols, etc. The paradigm of benign by design synthesis of nanomaterials was promoted in recent years in our aim to switch to more environmentally (bio)compatible materials and products with comparable efficiencies and cost-competitive with respect to current possibilities for a more sustainable society.[4]

Mechanochemistry recently emerged as a highly promising technology that makes use of the power of grinding/milling to promote chemical changes in the internal structures of materials.[5] The mechanochemical reaction happens through the fracturing of the original

structure of the starting materials that cause the incorporation of the new species within the lattice or the structure. Because of high energy collisions between reactants and/or solids, changes in materials can be promoted at much lower temperatures.[6] This non-traditional synthetic approach features an extreme simplicity, cleanliness, reproducibility and versatility, being already demonstrated to be highly useful for the development of a range of advanced nanomaterials including MOFs, supported metal and metal oxide nanoparticles and nanocomposites with diverse applications in catalysis, sensing, drug delivery and adsorption.[5, 7] Most importantly, the activities and specificities of mechanochemically synthesized materials have been extensively demonstrated to significantly predate those of conventionally synthesized materials in various applications including bio-compatibility studies.[7, 8]

Improved catalytic activities, conductivities, reactivities and related improved properties achieved in designer advanced nanomaterials can also be accompanied by altered interactions with biological systems at cellular level.[9] These unknown interactions can affect biological functions that would not otherwise be observed with bulk materials (not in the nano-range). In fact, recent studies on potential nanotoxicity to human health and the eco-environment have drawn the attention of both government agencies and the general public.[10, 11] Anumber of studies have recently shown that nanoparticles can contribute to adverse health effects which have been attributed to reactive oxygen species (ROS) generation. For example, cytotoxicity studies of TiO_2 nanoparticles demonstrate oxidative stress in various human cell lines such as human skin fibroblast cells[12] and human bronchial epithelial cells.[13] Moreover, genotoxicity studies in various cell lines have shown that nanoparticles could cause DNA damage and increase the mutation frequency.[14-15]

With the increasing presence of nanomaterials and nanoparticles in daily lifes and routine exposure to such nanoentities, the understanding of their interactions in human cells

as well as their toxicities are matter of utmost importance in scientific research. As examples, ZnO and TiO_2 nanoparticles are currently present in sunscreen formulations and other common applications where UV protection from transparent coating is required (e.g. creams, beauty treatments, varnishes to protect wood, etc.). [16-17] However, restricted studies are available on their interactions with the skin and/or human cells (e.g. migration to internal organs) during uptaking or after repeated/long-term exposure.

ZnO as well as TiO_2 nanoparticles have been extensively investigated in the field of photocatalysis[8d, 18]. Particularly ZnO nanoparticles have been demonstrated to be very toxic at moderate concentrations for a wide variety of biological systems including epidermal cells.[19] ZnO nanomaterials are also toxic to T cells at concentrations above 5 mM,[20] being toxic to neuroblastoma cells above 1.2 mM.[21]. Furthermore, ZnO nanoparticles were more cytotoxic to microorganisms such as *E. coli* as compared to other metal oxide nanoparticles such as Fe_2O_3, Y_2O_3, TiO_2 and CuO.[22] The plausible reason for the observed toxicity is that nanosized ZnO (similar to TiO_2) is an excellent photocatalyst that generates excessive ROS (reactive oxygen species) that can damage cellular proteins, lipids and DNA, leading to fatal cell lesions.[19] However, recent studies indicated that ZnO nanoparticles may also exhibit a preferential ability to kill cancerous cells as compared with normal line cells,[23] potentially emerging as a promising new modality of cancer therapy, the so-called photodynamic therapy (PDT). PDT promises a better selectivity for tumors that are accessible to light, low systemic toxicity, and fewer side effects in comparison to radiation therapy and chemotherapy.[24-25]

Based on these premises to improve the efficiency and biocompatibility of ZnO nanoparticles in view of potential biomedical applications, the proposed study was aimed to demonstrate an improved biocompatibility of novel ZnO-polysaccharide advanced

nanohybrids synthesized using a recently developed innovative mechanochemical protocol.[26] Polysaccharides extracted from fungal microorganisms were utilised both as nanoparticle carriers and sacrificial templates[27] to minimise Zn^{2+} release (related to cytotoxicity) as investigated in MTT assays (Scheme 1).

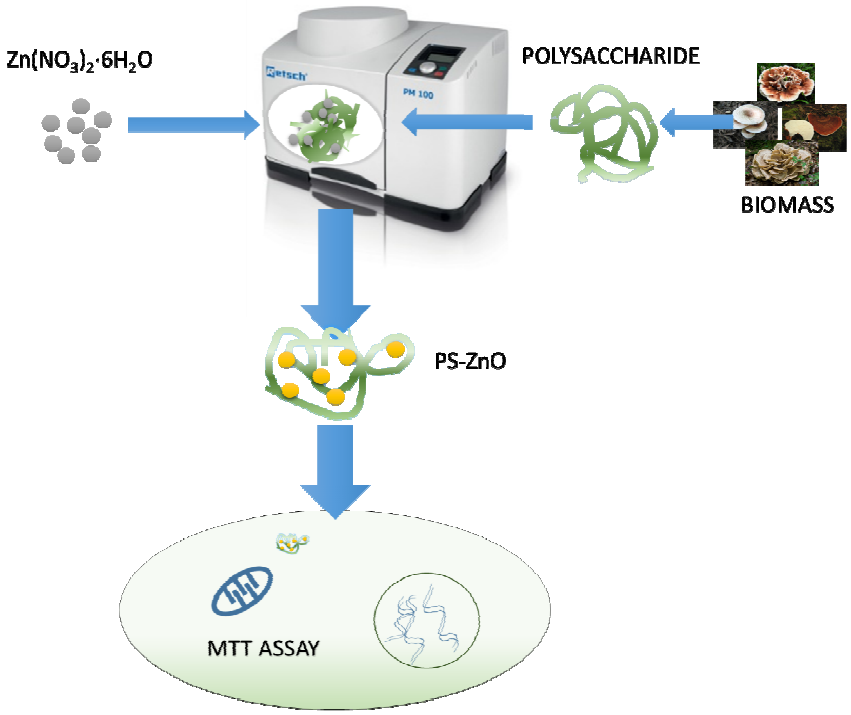

Scheme 1. Mechanochemical preparation of biocompatible PS-ZnO materials.

Experimental section

Synthesis of ZnO-polysaccharide nanohybrids

The preparation of ZnO-polyssacaride nanohybrids was carried out using a previously reported ball milling protocol.[26] Polysaccharides were obtained by extraction from different fungal microorganisms including *Abortiporus biennis* (PS1), *Lentinus tigrinus* (PS2), *Rigidoporus microporus* (PS5) and *Ginkgo polypore* (PS10), being some of these fungi autoctonous from China. In a typical experiment, the desired quantity of zinc precursor

[typically $Zn(NO_3)_2 \cdot 6H_2O$] was ground with a certain quantity of polysaccharide at 2:1 zinc precursor/polysaccharide w/w ratio in a 125 mL stainless recipient of a Retsch-PM100 planetary ball mill at 350 rpm for 30 min (optimized conditions). Eighteen stainless steel balls of 1 cm diameter were employed. Upon milling, the obtained jelly-like materials were oven-dried for 24 h. After powderising, the dried solids were transferred to ceramic vessels and subsequently calcined in air at 600 ºC for 3 h in order to remove the unbound organic compounds. The obtained materials were labelled according to the type of polysaccharides used as PS1-ZnO, PS2-ZnO, PS5-ZnO and PS10-ZnO.

Materials characterisation

The structure regularity of the samples was determined by XRD on a Siemens D-5000 (40 kV, 30 mA) using Cu Kα (λ=0.15418 nm) radiation. Scans were performed over a 2 θ range from 10 to 80 at step size of 0.018 º, with a counting time per step of 20 s.

Nitrogen adsorption measurements were carried out at 77º K using an ASAP 2000 volumetric adsorption analyser from Micromeritics. Samples were degassed for 24 h at 150ºC under vacuum ($p < 10^{-2}$ Pa) prior to adsorption measurements. Surface areas were calculated according to the BET (Brunauer-Emmet-Teller) equation. Pore volumes (VBJH) and pore size distributions (DBJH) were obtained from the N_2 desorption branch.

The size and morphology of carbonaceous materials were investigated using a Electron Microscopy. Scanning Electron Microscopy (SEM) and elemental analysis were recorded on a JEOL 173 JSM-6300 Scanning Microscope with energy dispersive X-ray analysis (EDX) at 20 kV. Samples were coated with Au/Pd on a high resolution sputtering SC7640 instrument at a sputtering rate of 1.5 kV per minute, up to 7 nm 177 thickness.

Transmission Electron Micrographs (TEM) were recorded on a JEOL JEM-2010HR instrument operated at 300 kV. Samples were suspended in ethanol and deposited straightaway on a copper grid prior to analysis.

DRIFT experiments were conducted in an FTS 6000 Bio-Rad instrument with a resolution up to 0.15 cm^{-1}. Spectra were scanned at room temperature in transmittance mode over the wavenumber range of 4000–650 cm^{-1}, with a scan speed of 0.20 209 cm s^{-1} and 30 accumulations at a resolution of 4 cm^{-1}. A background spectrum of air was scanned under the same instrumental conditions before each series of measurements.

Thermal analysis was performed by simultaneous thermal gravimetric and differential thermal analysis (TG-DTA) measurement using a Setsys 12 Setaram thermobalance and α-Al_2O_3 as the reference material, and a Pt/Pt-Rh (10%) thermopar for temperature control. Samples were heated in air (50 mL min^{-1}) at 30–900 °C of temperature range and at a heating rate of 10 °C min^{-1}.

XPS measurements were performed in an ultra-high vacuum (UHV) multipurpose surface analysis system (SpecsTM model, Germany) operating at pressures of $<10^{-10}$ mbar using a conventional X-ray source (XR-50, Specs, Mg K, 1253.6 eV) in a "stop-and-go" mode to reduce potential damage due to sample irradiation. The survey and detailed Fe and Cu high- resolution spectra (pass energy 25 and 10 eV, step size 1 and 0.1 eV, respectively) were recorded at room temperature with a Phoibos 150-MCD energy analyser. Powdered samples were deposited on a sample holder using double-sided adhesive tape and subsequently evacuated under vacuum ($<10^{-6}$ Torr) overnight. Eventually, the sample holder containing the degassed sample was transferred to the analysis chamber for XPS studies.

Cell cultures

The two human cell lines used in this study (A549 and SH-SY5Y) were obtained from American Type Culture Collection (Manassas, VA, USA). A549 lung adenocarcinoma cell line was grown in Ham's F-12K (Kaighn's) medium. In turn, SH-SY5Y neuroblastoma cell line was grown in MEM nutrient medium, supplemented with 1% MEM non-essential amino acids and L-glutamine (2 mM). The media for both cell lines were supplemented with 10% (v/v) fetal bovine serum, 10 units mL^{-1} penicillin, and 100 mg mL^{-1} streptomycin. Cells were grown at 37ºC in a humidified incubator with 5% CO_2 and 95% air.

Cell treatments and measurement of cell viability

Cell viability was colorimetrically quantified using the metabolic dye MTT. When cultures were confluent (70-80 %), cells were seeded in 96-well tissue culture plates at density of 1×10^4 cells/well in complete medium. After 24 h of cell attachment, the cells were exposed to ZnO-polysaccharide materials (suspended in deionized water using sonication for 15 minutes in an ice bath) at final concentrations between 10 and 400 µg mL^{-1} for 24, 48 or 72 h at 37 ºC. MTT was added to the cells 3 h. prior to the end of the experiment at a final concentration of 0.5 mg mL^{-1}. During that time, MTT was reduced to produce a dark blue formazan product. The medium was then removed, with cells dissolved in DMSO. Formazan production was measured by the change in absorbance at 595 nm using a microplate reader (BioTek Power Wave XS). The viability results were expressed as a percentage of control (untreated cells). EC50 (50% effective concentration) was computationally calculated using GraphPad Prism v4.0 for Windows (GraphPad Software, San Diego CA, USA; http://www.graphpad.com).

Statistical analysis

Levene's test of homogeneity was applied to test the variance of the data. After testing the normality and homogeneity of variances, statistical significance was assessed by one-way ANOVA, followed by a Tukey *post hoc* test. Statistical analyses were carried out using the version 19 of SPSS (SPSS Sciences, Chicago, Illinois). Significance was defined as a p value less than 0.05. Results are displayed as mean values ± SD for at least four independent experiments.

Dissolved zinc concentrations in the cell culture medium

To examine the dissolution of the different types of ZnO-polysaccharide nanohybrids in cell culture media, the concentrations of zinc ions released from ZnO-NPs were quantified using inductively-coupled-plasma mass-spectrometry (ICP-MS).

Firstly, concentrations of different ZnO-polysaccharide nanohybrid (10, 100 and 200 µg/mL for Ham's F-12K medium and 10, 50 and 100 µg/mL for MEM nutrient medium, respectively) were dispersed in 10 % FBS supplemented media and further incubated during 24 h in 5% CO_2 at 37 °C with 95% humidity. Aliquots (1 mL) were then withdrawn, centrifuged (15,000g, 20 min) and supernatants were introduced in a microsampling quartz insert, using 10 % nitric acid (Suprapur, E. Merck) to digest the samples. The microsampling inserts were then introduced in Teflon vessels and put into a microwave oven Star D (Milestone, Sorisole, Italy).[28]

All materials were previously washed with 10% nitric acid in order to avoid any potential contamination. Zn concentrations were determined by means of a computer-controlled sequential ICP-MS (Perkin Elmer Elan 6000) according to DIN EN ISO

17294-2. The detection limit, which was calculated as three times the standard deviation of the blank signal, was 0.02 µg/mL for Zn.

Results and discussion

Surface areas of synthesized materials (Table 1) were in the range of 15-20 $m^2 g^{-1}$, with a pore diameter from 20 to 28 nm. Results indicate that some mesoporosity was developed in the mechanochemically synthesized materials after calcination, with only subtle differences between PS1 and PS10-ZnO nanohybrids in terms of textural properties. These differences could be due to the more defined internal structure of ZnO materials.[29] The internal crystalline structures of the nanohybrids are not entirely consistent with those reported in literature[30], most probably due to layer stacking of the crystal structure of incorporated ZnO within the polysaccharide matrix.[8d]

DRIFT Spectra of ZnO-polysaccharide nanohybrids clearly show the incorporation of the metal into the structure of the polysaccharide considering the calcinations step (Figure 1). This step was performed to remove unbound organic compounds for the design of the ZnO nanohybrids. The apparent presence of –OH (~3500 cm^{-1}) and C=C (~2300 cm^{-1}) bonds in the materials corresponds to the complexation of Zn with these functional groups, to form strongly coordinated covalent bonds which were not removed under slow heating during calcination.[31] C content in ZnO nanohybrids is under 10% (as determined by elemental analysis), also unique in these type of nanomaterials. These results also confirmed the occurrence of a mechanochemical reaction between polysaccharides and the Zn precursor, in good agreement with previous reports and confirmed in the Zn^{2+} concentration/determination experiments.[5, 7,8]

Table 1. Textural properties of synthesized ZnO-polysaccharide nanohybrids.

Material	S_{BET}[a] (m^2g^{-1})	D_{BJH}[b] (nm)	V_{BJH}[c] (cm^3g^{-1})
PS1-ZnO	18	28	0.12
PS2-ZnO	15	19	0.06
PS5-ZnO	16	21	0.08
PS10-ZnO	20	28	0.13

[a]S_{BET}: specific surface area was calculated by the Brunauer-Emmett-Teller (BET) equation. [b]D_{BJH}: mean pore size diameter was calculated by the Barret-Joyner-Halenda (BJH) equation. [c]V_{BJH}: pore volumes were calculated by the Barret-Joyner-Halenda (BJH) equation.

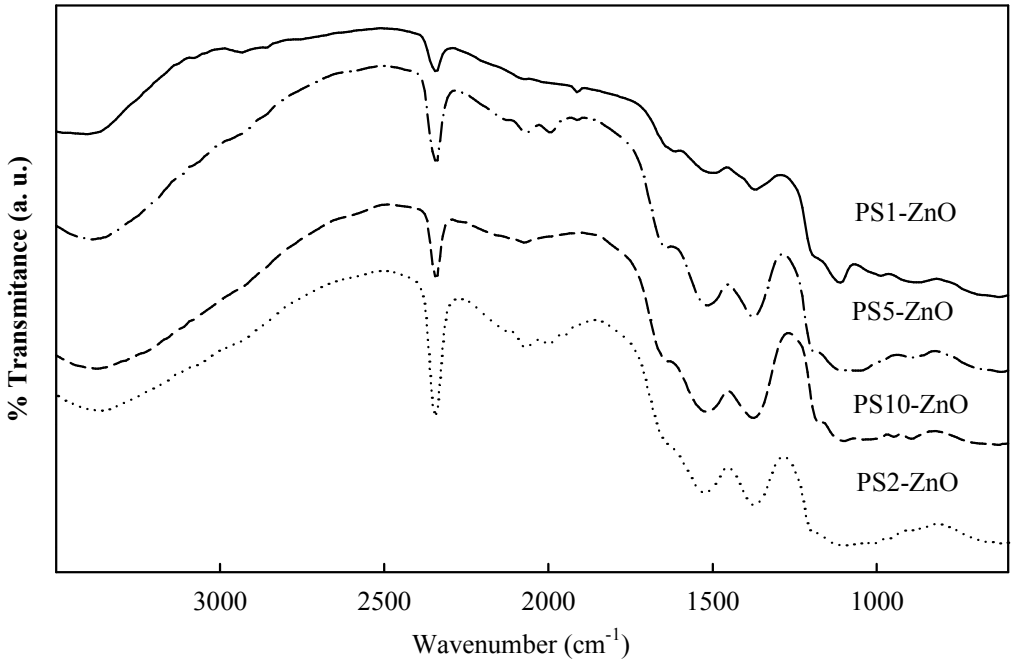

Figure 1. DRIFT spectra of ZnO-polysaccharide materials.

The presence of other groups including C-O and C=O can be also hinted from the spectra, oxidized species that may have formed during the ball-milling step and/or during the heat treatment (calcinations) in air at 600ºC. On one hand, dehydration reactions within the polysaccharide can also explain the presence of a large amount of water formed after the mechanochemical process (a jelly-like wet material was obtained upon milling).[32]

Additionally, the change in colour of the materials from white to grey-ish may also indicate the formation of new chemical species via mechanochemistry.

SEM micrographs included in Figure 2 depicted no significant differences in terms of morphology between different synthesized materials. These nanohybrids exhibited a porous and fibrous-like particulate morphology with a number of large particle sizes (10-50 μm, Figure 2D) which seem to be present as aggregates of small material bits with an interesting similar roughness to previously reported alginic acid and starch biotemplated ZnO.[8d] The observed morphology is a consequence of the milling technique which is known to cause a deformation and/or exfoliation/breaking down of microparticles to smaller nanoparticles under different conditions.

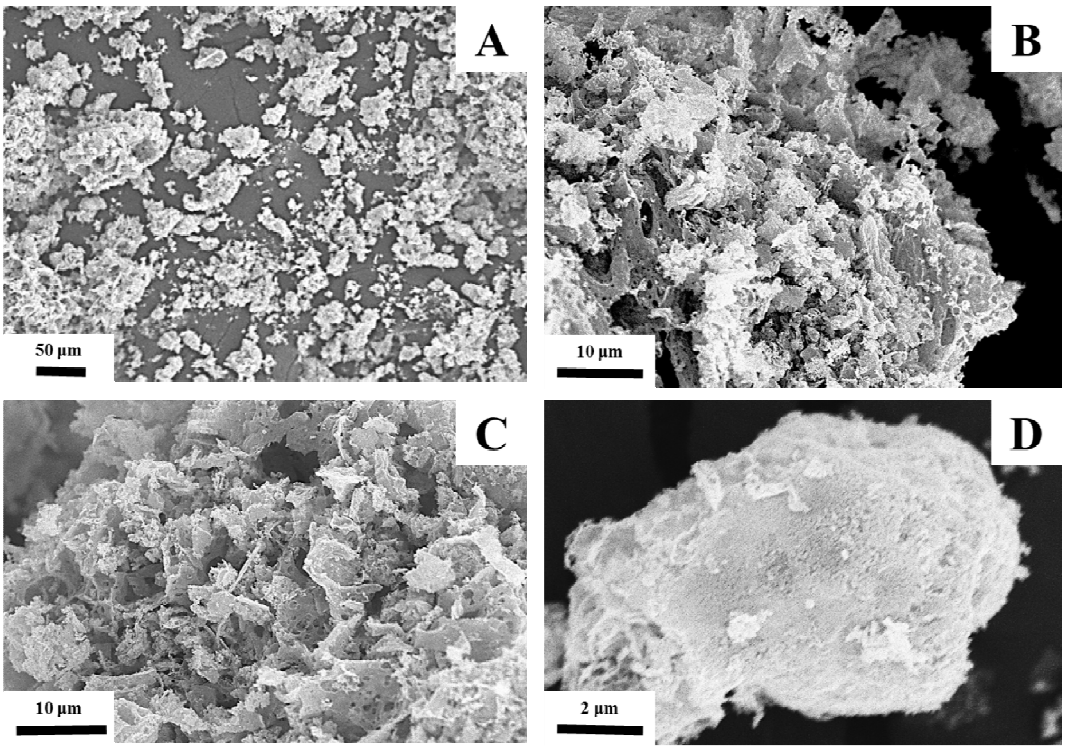

Figure 2. SEM micrographs of (A) PS1-ZnO; (B) PS2-ZnO; (C) and (D) PS5-ZnO.

X-ray diffraction (XRD) was utilised to assess the crystal structure and size of prepared ZnO-polysaccharides nanohybrids. Figure 3 depicts the diffraction patterns of

different PS-ZnO materials. All patterns have characteristic diffraction lines corresponding to a wurtzite crystal structure (Zincite, #36-1451),[33] verifying that all ZnO-polysaccharides nanomaterials have an extremely similar and high crystallinity. Interestingly, the unite cell was found to be significantly reduced (a=2.79; c=4.48 A) as compared to typical wurtzite ZnO (a=3.24; c=5.20 A) which supported the observations by DRIFTs, SEM and TEM of the differences between literature ZnO materials and present mechanochemically synthesized nanohybrids. The average nanoparticle crystal size for the samples were ~30 nm as was estimated using the Scherrer's equation.[34] Additional diffraction lines could be observed in the XRD pattern (e.g. 2 theta= 32 and 47) which correspond to additional phases present in the materials from the polysaccharide impurities (results not shown) including Ca, Si and Al.

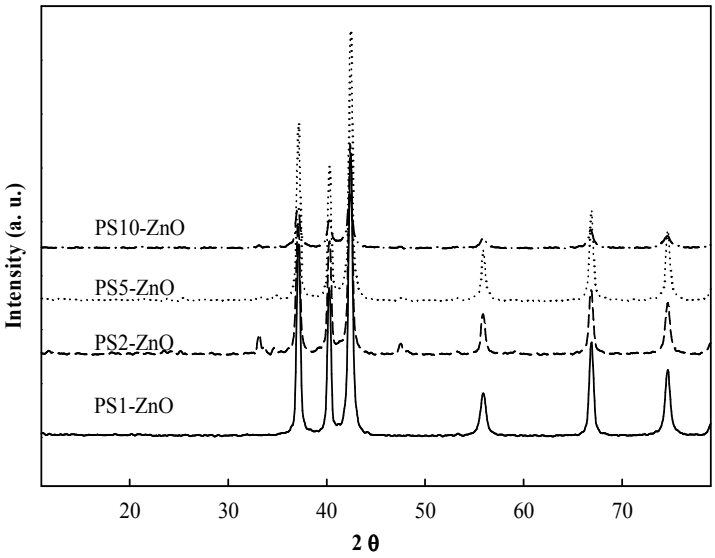

Figure 3. X-ray diffraction patterns of PS-ZnO materials.

The calculated average crystal size by XRD was in good agreement with TEM micrographs of the ZnO nanomaterials as visualised in Figure 4. TEM images proved the presence of homogeneously distributed nanocrystals in the materials, with nanocrystal diameters generally between 20 to 40 nm in size (Figure 4B and C). In most cases, the porous and fibrous morphology of particles observed by SEM was also clearly visualised in TEM

images, although alternative nanocrystal structures (i.e. tubular nanostructures) could be occasionally observed in some materials (Figure 4) depending on the parent polysaccharide utilised as template. EDX analysis of investigated materials proved a significant content of C present in the materials despite the high temperature calcinations step (between 5-10% in weight, 12 to 18% atomic) together with Zn and O. PS1-ZnO possessed the lowest C concentration in the samples (ca. 5 wt.%) as compared to the highest C content determined for PS10-ZnO (ca. 9.8 wt.%), with PS5 and PS2 to be found in between those limits.

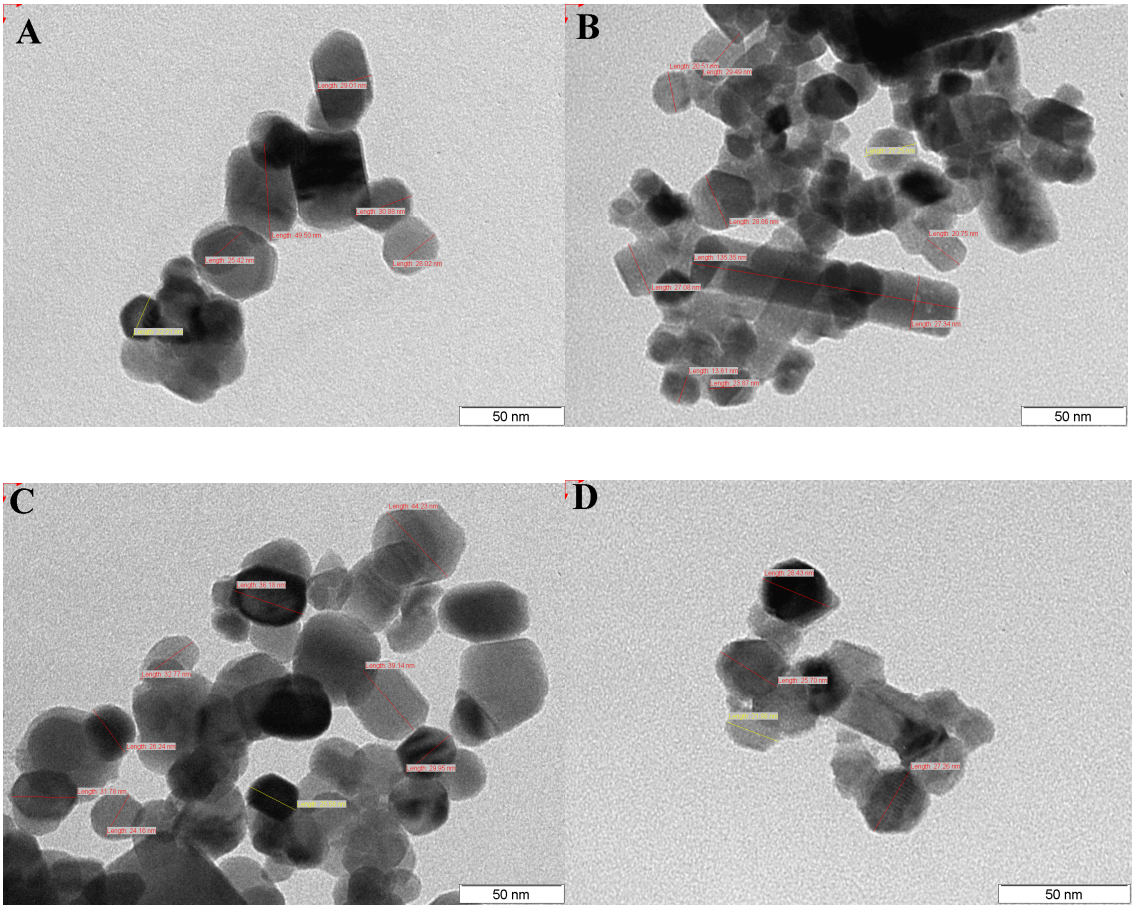

Figure 4. TEM images at different magnifications of A) PS1-ZnO (with measured nanoparticle sizes); B) PS2-ZnO; C) PS5-ZnO and D) PS10-ZnO which illustrate the relatively homogeneous nature of the nanomaterials in terms of nanoparticle size and distribution.

Importantly, the presence of unremoved C species from the polysaccharides upon heating at 600ºC may support the mechanochemical reaction between functional groups of polysaccharides (e.g. carboxyl, hydroxyl) with the Zn precursor. Traces of other elements including Ca, Al, Si and Cl could also be detected in the final PS-ZnO materials. However, the content of these elements was found to be under 2 wt% (typically 0.5-1.8 wt.%). Based on these findings, the content of ZnO in the materials was quantified to be between 88% and 94%, essentially containing 5-10% lower purity as compared to commercial pure ZnO materials.

Thermogravimetric results of uncalcined nanohybrids have been depicted in Figure 5. There were not significant differences between synthesized materials. A rather large mass loss is clearly visible under 300 ºC which could be due to the removal of the unbound organic part of the polysaccharide, accompanied by an endothermic peak at 100 ºC due to elimination of physisorbed or occluded water within the pores of the materials. TGA analysis also confirmed the presence of C (ca. 25-30%) from the different mass losses at temperatures over 200ºC as indicated by TGA-MS (results not shown).

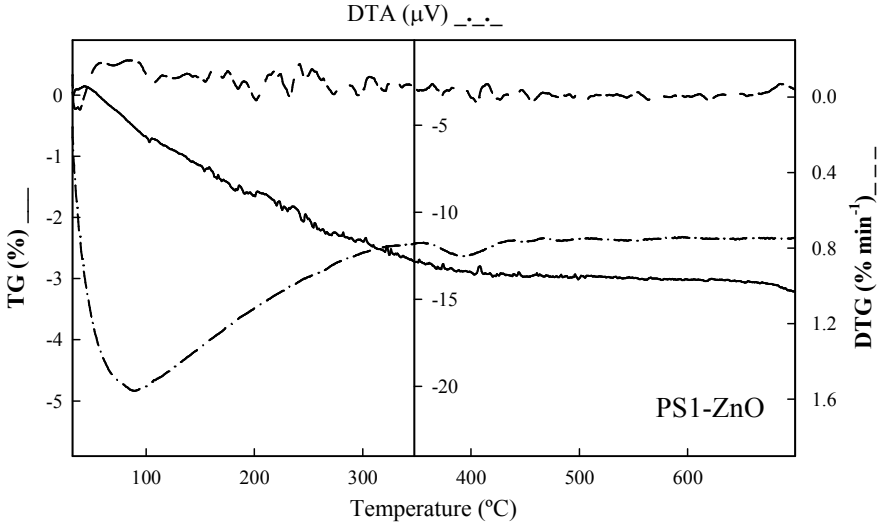

Figure 5. TG-DTA profiles of PS1-ZnO.

Importantly, there was almost no mass loss in the materials after 400-500ºC despite the observed C content of 5-10 wt.% in final calcined materials at 600ºC. These interesting findings are also in good agreement with the proposed mechanochemical reaction between functional groups of the polysaccharide and the Zn precursor, further confirmed by the low release of Zn^{2+} ions for certain PS-ZnO nanohybrids (e.g. PS10-ZnO).

XPS spectra of various polysaccharide-metal hybrid materials are depicted in Figure 6. C1s spectra mainly show the presence of both C-C (285 eV) and C-O (286 eV) species in the surface of the materials. These carbons species are consistent with the presence of C-containing functional groups of polysaccharides on the surface, in good agreement with previous TGA and DRIFT results. The presence of these remaining C-containing functionalities even after materials calcination at 600ºC again support the suggested mechanochemical reaction in the preparation of the materials which led to highly stable C-containing ZnO nanohybrids. Oxidised carbon species can be also observed in peaks at ~292 eV. [35-36] The positions of the peaks for carbon are also consistent with values reported for aromatic materials and graphene. However, evidences derived from other characterisation techniques do not suggest the presence of these species. Figure 6 also shows the spectra of O1s, confirming the presence of oxygen in the surface associated with C-O bonds.[35] In the case of the Zn 2p spectra, two interesting peaks were found. The peak at ~1022 eV (for some materials ~1028 eV) corresponds to $Zn2p_{3/2}$ (contribution from ZnO) as commonly reported in literature[37], with the second peak at much higher binding energies corresponding to $Zn2p_{1/2}$.[38] The peak distance between these two peaks is a signature of the presence of ZnO nanoparticles,[39] in good agreement with XRD data.

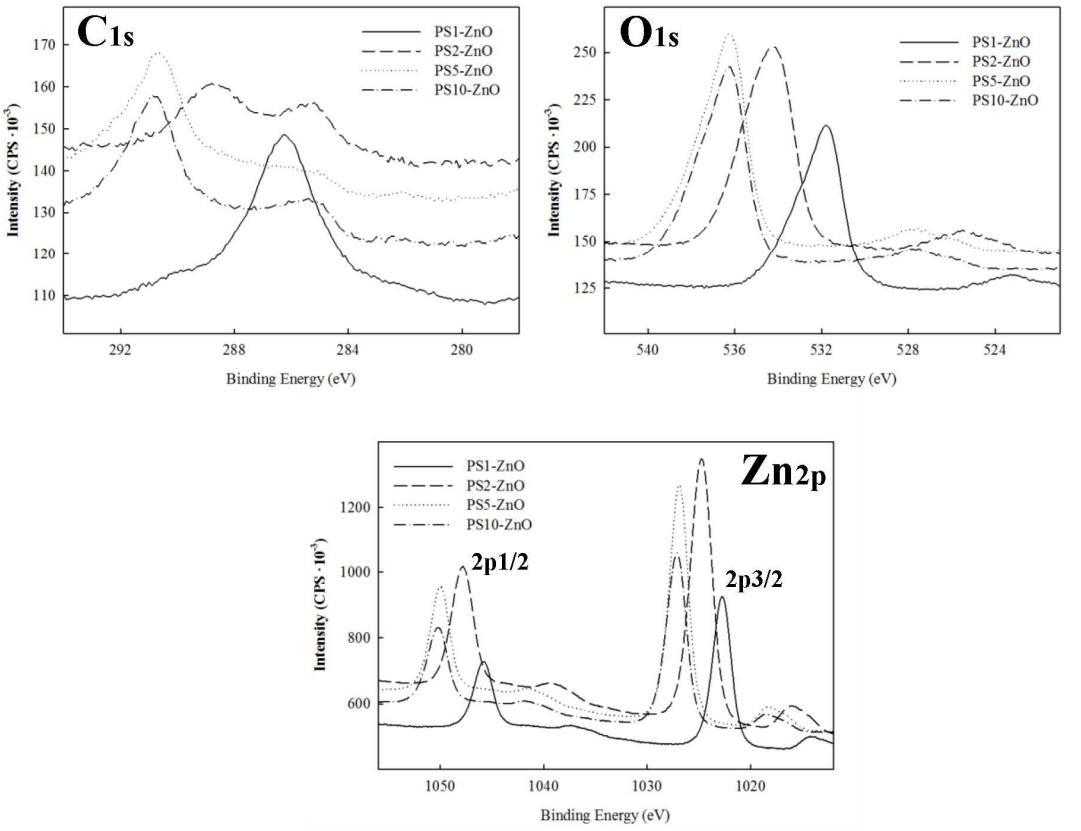

Figure 6. XPS spectra of different ZnO-polysaccharide hybrid materials.

Toxicity studies of ZnO-polysaccharides nanohybrids in human carcinoma cells

Upon materials characterisation, ZnO nanohybrids were subsequently evaluated in a number of toxicity studies. Cell viability was assessed by the MTT assay, which measures mitochondrial reductase activity. The cytotoxicity effects to increasing concentrations of PS-ZnO nanohybrids (10-200 μg mL^{-1}) after 24 h of exposure have been summarised in Figure 7. Interestingly, PS-ZnO materials induced very unique dose dependent cytotoxic effects on both SH-SY5Y and A549 cells, being only statistically significant ($p < 0.001$) at concentrations higher than 50 μg mL^{-1}, as compared to their respective control experiments.

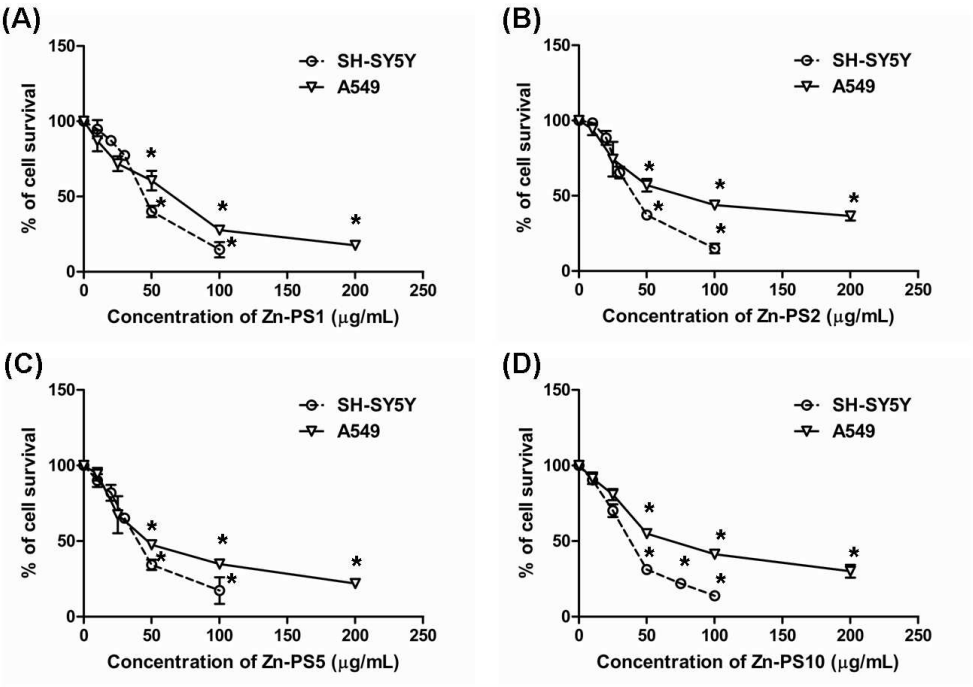

Figure 7. Viability percentage measured by MTT assay on A549 and SH-SY5Y cell lines exposed to 10-200 μg mL^{-1} of different PS-ZnO nanohybrids (A: PS1-ZnO, B: PS2-ZnO, C: PS5-ZnO, and D: PS10-ZnO) for 24 h. An OD value of control cells (unexposed cells) was considered as 100% viability (negligible cytotoxicity). Data were reported as mean values ± SD of three independent experiments (an asterisk indicates significant different from control: $p < 0.001$).

No significant differences were noted among EC50 values (the effective concentration causing 50 % of maximum effect) obtained from different treatments of PS-ZnO materials for each cell line (Table 2). Unexpectedly, A549 cells were also less susceptible to PS-ZnO treatment with respect to SH-SY5Y cells, showing EC50 values greater to those of SH-SY5Y. EC50 values for SH-SY5Y cells were all approximately 50 μg mL^{-1}, while for A549 cells were 100 μg mL^{-1}, both unprecedented in similarly reported 20-30 nm ZnO literature nanomaterials, most observed under 25 μg mL^{-1} (Table 3).[40-42]

Table 2. Effective concentration causing 50% maximum effect (EC50) in two different cell lines after exposure to PS1-ZnO, PS2-ZnO, PS5-ZnO and PS10-ZnO NPs for 24 hours.

Cell lines	EC50 (μg mL^{-1}) based on MTT assay			
	PS1-ZnO	PS2-ZnO	PS5-ZnO	PS10-ZnO
A549	90.8 ± 4.8	121.8 ± 10.2	93.6 ± 6.4	112.3 ± 2.1
SH-SY5Y	53.4 ± 4.5	50.21 ± 0.6	49.1 ± 5.6	48.3 ± 0.8

Results as expressed as mean values ± SD, of four independent replicate experiments performed for each cell line.

Table 3. A comparison between PS-ZnO materials and literature data for materials cytotoxicity (expressed as EC50, ZnO dosage) for A549 cells after exposure for 24 hours.

Materials	Preparation conditions	Particle size (nm)	EC50 (μg mL^{-1})	Reference
NanoZnO	Solvothermal process, zinc acetate as precursor	15-48	8-10	42
nZnO	Uncoated commercial ZnO powder	20-30	[a]	46
Nano ZnO	Coprecipitation of zinc acetate dehydrate in NaOH	30	15	47
Nano ZnO[b]	Uncoated commercial ZnO powder	20-30	15-20	48
Nano ZnO	Uncoated commercial ZnO powder	50-70	<20	49
Micro-ZnO	Uncoated commercial ZnO powder	<1,000	<20	49
Nano ZnO	Commercial ZnO treated with H_2O_2	14-98	<50	50
PS2-ZnO	Mechanochemical, fungal polysaccharides + Zn precursors	30	110-130	This work

[a]Acute cytotoxicity was developed within 1.5 h (100 μg mL^{-1} nZnO treatment).

[b]Data from experiments showed that 26-nm ZnO NPs appeared to have the highest toxicity for Caco-2 cells.

Furthermore, some differences could be particularly observed for materials PS2-ZnO (from *Lentinus tigrinus) and* PS10-ZnO *(from Ginkgo polypore*) in terms of a markedly low toxicity for A549 cells. Polysaccharides extracted from such fungi species have not been fully characterised but the differences in toxicity as well as the unprecedently observed low toxicity of PS-ZnO nanohybrids has been proved to be due to the low solubility of ZnO which results in a lower release of free intracellular Zn^{2+}. ICP-MS measurements of the soluble zinc supernatant of PS-ZnO nanohybrids dispersions in supplemented cell culture media summarised in Table 4 support these claims. Released Zn^{2+} concentration values were found to be relatively similar for most PS-ZnO nanohybrids at the same concentrations, with the exception of PS1-ZnO in A549 cell culture medium, which was twice as high with respect to average values obtained for PS-ZnO nanohybrid samples at 200 μg/mL (ca. 66 μg/mL vs typically 26-30 μg/mL, Table 4) and PS10-ZnO which generally exhibited reduced Zn^{2+} concentrations as compared to the remaining nanohybrids.

Remarkably, concentrations of zinc released were significantly higher in A549 cell culture medium with respect to SH-SY5Y medium, particularly at higher dosages of PS-ZnO. In any case, PS10-ZnO exhibited the lowest zinc release in both mediums while PS1-ZnO and PS5-ZnO presented a high zinc release in A549 and SH-SY5Y cell culture medium, respectively. These values of Zn^{2+} release correlate well with the presence of C content in the nanohybrids, with PS10-ZnO and PS2-ZnO (higher C content) exhibiting an unprecedently low toxicity associated to a reduced Zn^{2+} release in such materials (Tables 3 and 4). An increase of Zn^{2+} concentration can be correlated to reduced cell viability (increased toxicity). Zn is a component of many enzymes (e.g., alcohol dehydrogenase, matrix metalloproteinase) and transcription factors (eg, zinc finger protein transcription factors). Consequently, disruption of cellular Zn homeostasis has been linked to cytotoxicity, oxidative stress, and mitochondrial dysfunction.[43-45] The porous nature of PS-ZnO nanohybrids as well as its C

content in mechanochemically synthesized materials reduces the release of Zn^{2+} ions as compared to any commercial nano ZnO systems.

Table 4. Analysis of released Zn (II) ions in cell culture media from ZnO polysaccharide nanohybrids.

A549 Cell Culture Media			
PS-ZnO nanohybrid concentration in experiment	**10 µg/mL**	**100 µg/mL**	**200 µg/mL**
Zn (II) release (µg/mL) from PS1-ZnO	6.6 ± 0.7	31.9 ± 0.3	66.7 ± 5.3
Zn (II) release (µg/mL) from PS2-ZnO	7.5 ± 0.7	29.2 ± 1.4	29.2 ± 1.0
Zn (II) release (µg/mL) from PS5-ZnO	8.9 ± 0.9	28.2 ± 2.1	33.7 ± 0.5
Zn (II) release (µg/mL) from PS10-ZnO	5.8 ± 1.1	20.6 ± 4.5	26.8 ± 0.1
SH-SY5Y Cell Culture Media			
PS-ZnO nanohybrid concentration in experiment	**10 µg/mL**	**50 µg/mL**	**100 µg/mL**
Zn (II) release (µg/mL) from PS1-ZnO	7.2 ± 0.8	13.5 ± 0.6	15.1 ± 1.6
Zn (II) release (µg/mL) from PS2-ZnO	6.3 ± 0.6	14.3 ± 0.7	14.2 ± 1.0
Zn (II) release (µg/mL) from PS5-ZnO	8.3 ± 0.9	14.5 ± 1.4	17.1 ± 2.8
Zn (II) release (µg/mL) from PS10-ZnO	4.7 ± 0.6	11.9 ± 0.1	13.3 ± 1.4

Results are presented as mean ± SD *(n=3)*.

Interestingly, results obtained for Zn^{2+} release in MEM medium were lower as compared to Ham's F-12K medium (see experimental). The observed differences can be attributed to the distinct composition between both media. Buffer solutions and cell culture media contain phosphate ions able to destroy ZnO nanoparticles within a time span from less than one hour to one day[51]. Solubility of ZnO nanomaterials can be also affected by various physical properties including particle size, specific surface area and surface modification. Our results (Table 4) are somehow similar to those previously reported in literature[52-55]although

Zn^{2+} release was particularly reduced in PS10-ZnO (nanohybrid containing the highest C content). A549 cells exposed to 100 μg/mL of PS10-ZnO produced a release of Zn^{2+} of ca. 26.8 μg/mL, leading to a decrease of cell viability of approx. 65%. Comparatively, the closest literature studies by Fukui *et al*. reported an over 80 % decrease in cell viability upon exposure of A549 cells to a concentration of 20 μg/mL of Zn^{2+} ions (30% inferior to that of the present study).[52]

Another additional reason for the decrease in the cytotoxicity of the ZnO nanohybrids may be related with a decrease in NP-cell contact, which decreases reactive oxidized species (ROS) production and protection of the membrane integrity.[43-45] This might also relate to the surface functionalities in PS-ZnO materials (OH, C-O, C-C and C=C bonds) as compared to conventionally synthesized ZnO nanomaterials which together with the C content can potentially confer a higher stability to PS-ZnO nanohybrids in cell culture media with the observed reduced release of Zn^{2+} ions.

Further studies are currently ongoing using dermal cell lines to ascertain whether the observed low cytotoxicity can be also extended to different types of cell lines, of particular interest to the development of highly effective, biocompatible UV blocking formulations (e.g. sunscreens).[17b]

Conclusions

In this study, polysaccharide-ZnO nanohybrids were synthesized using a reactive milling protocol under mild conditions with low-toxicity at high concentrations. Characterisation studies showed that C-containing ZnO nanomaterials were formed after the mechanochemical process, forming mesoporous nanomaterials (ca. 15-20 m^2g^{-1}) with nanoparticle sizes of ca. 30 nm. Remarkably, the synthesized bio-inspired nanomaterials exhibited an unprecedented

cytotoxicity for human cell lines (A549 and SH-SY5Y) at high ZnO concentrations (>100 μg mL^{-1}) as compared to the best to date reported ZnO nanomaterials. The reasons for the low cytotoxicity essentially relate to the low release of ZnO in PS-ZnO nanohybrids (with Zn^{2+} being slowly released into solution) as well as the reduced interaction NPs-cells due to the different surface functionalities present in the PS-ZnO nanohybrids as confirmed by XPS, DRIFTs and related techniques. However, NPs of different chemical compositions and properties follow different uptake pathways and employ different mechanisms toward their final biological responses, hence being difficult to determine toxicity profiles based on a single type of NP. Further studies are currently ongoing with different types of nanoparticles (e.g. Ag and AgO) as well as various parameters (i.e. nanoparticle sizes, crystalline structure, shapes, etc.) to provide additional insights into nanomaterials interaction with cell membranes and organelles as well as their transport mechanisms in cells.

Acknowledgments

Rafael Luque gratefully acknowledges Spanish MICINN for financial support via the concession of a RyC contract (ref: RYC-2009-04199) and funding under project CTQ2011-28954-C02-02 (MEC). Consejeria de Ciencia e Innovacion, Junta de Andalucia is also gratefully acknowledged for funding project P10-FQM-6711.

References

(1) Huebsch, N.; Mooney, D. J. Inspiration and application in the evolution of biomaterials. *Nature* **2009**, *462* (7272), 426–432.

(2) Li, J. W. H.; Vederas, J. C. Drug discovery and natural products: End of era or an endless frontier? *Biomeditsinskaya Khimiya* **2011**, *57* (2), 148–160.

(3) Patete, J. M.; Peng, X.; Koenigsmann, C.; Xu, Y.; Karn, B.; Wong, S. S. Viable methodologies for the synthesis of high-quality nanostructures. *Green Chemistry*. **2011**, *13* (3), 482-519.

(4) a) G.A. Ozin, A.C. Arsenault, L. Cademartiri, Nanochemistry: A Chemical Approach to Nanomaterials. 2nd edition, RSC, Cambridge, UK, 2008; b) R. Luque, R.S. Varma, Sustainable preparation of nanoparticles RSC Green Chemistry Book series, Cambridge, UK, 2012; c) Murphy, C. J. Sustainability as an emerging design criterion in nanoparticle synthesis and applications. *Journal of Materials Chemistry* **2008**, *18*, 2173-2176.

(5) James, S. L.; Adams, C. J.; Bolm, C.; Braga, D.; Collier, P.; Friscic, T.; Grepioni, F.; Harris, K. D. M.; Hyett, G.; Jones, W.; et al. Mechanochemistry: opportunities for new and cleaner synthesis. *Chem. Soc. Rev.* **2012**, *41*, 413–447.

(6) Tsuzuki, T.; McCormick, P. G. Mechanochemical synthesis of nanoparticles. *J. Mater. Sci.* **2004**, *39* (16-17), 5143-5146.

(7) a) Beldon, P. J.; Fábián, L.; Stein, R. S.; Thirumurugan, a.; Cheetham, A. K.; Friščić, T. Rapid room-temperature synthesis of zeolitic imidazolate frameworks by using mechanochemistry. *Angew. Chemie - Int. Ed.* **2010**, *49* (50), 9640–9643; b) Yuan, W.; Friščič, T.; Apperley, D.; James, S. L. High reactivity of metal-organic frameworks under grinding conditions: Parallels with organic molecular materials. *Angew. Chemie - Int. Ed.* **2010**, *49* (23), 3916–3919; c) Friščić, T.; Halasz, I.; Beldon, P. J.; Belenguer, A. M.; Adams, F.; Kimber, S. a J.; Honkimäki, V.; Dinnebier, R. E. Real-time and in situ monitoring of mechanochemical milling reactions. *Nat. Chem.* **2013**, *5* (1), 66–73.

(8) a) Siamaki, A. R.; Lin, Y.; Woodberry, K.; Connell, J. W. and Gupton, B. F.Palladium Nanoparticles Supported on Carbon Nanotubes from Solventless Preparations: Versatile Catalysts for Ligand-Free Suzuki Cross Coupling Reactions. *J. Mater. Chem. A.* **2013***, 1,* 12909-12915; b) Rak, M. J.; Saadé, N. K.; Friščić, T.; Moores, A. Mechanosynthesis of ultra-small monodisperse amine-stabilized gold nanoparticles with controllable size. *Green Chem.* **2013**, *16* (1), 86–89. c) Kondrat, S. a.; Shaw, G.; Freakley, S. J.; He, Q.; Hampton, J.; Edwards, J. K.; Miedziak, P. J.; Davies, T. E.; Carley, A. F.; Taylor, S. H.; et al. Physical mixing of metal acetates: a simple, scalable method to produce active chloride free bimetallic catalysts. *Chemical Science* **2012**, *3* (10), 2965–2971. d) Francavilla, M.; Pineda, A.; Romero, A. a.; Colmenares, J. C.; Vargas, C.; Monteleone, M.; Luque, R. Efficient and simple reactive milling preparation of photocatalytically active porous ZnO nanostructures using biomass derived polysaccharides. *Green Chem.* **2014**, *16* (5), 2876-2885.

(9) Arancon, R. A. D.; Lin, S. H. T.; Chen, G.; Lin, C. S. K.; Lai, J.; Xu, G.; Luque, R. Nanoparticle tracking analysis of gold nanomaterials stabilized by various capping agents. *RSC Adv.* **2014**, *4* (33), 17114-17119.

(10) Oberdörster, G.; Oberdörster, E.; Oberdörster, J. Nanotoxicology: An emerging discipline evolving from studies of ultrafine particles. *Environ. Health Perspect.* **2005**, *113* (7), 823–839.

(11) Nel, A.; Xia, T.; Mädler, L.; Li, N. Toxic potential of materials at the nanolevel. *Science* **2006**, *311* (5761), 622–627.

(12) Wamer, W. G.; Yin, J. J.; Wei, R. R. Oxidative damage to nucleic acids photosensitized by titanium dioxide. *Free Radic. Biol. Med.* **1997**, *23* (6), 851-858.

(13) Gurr, J. R.; Wang, A. S. S.; Chen, C. H.; Jan, K. Y. Ultrafine titanium dioxide particles in the absence of photoactivation can induce oxidative damage to human bronchial epithelial cells. *Toxicology* **2005**, *213* (1-2), 66–73.

(14) Trouiller, B.; Reliene, R.; Westbrook, A.; Solaimani, P.; Schiestl, R. H. Titanium dioxide nanoparticles induce DNA damage and genetic instability in vivo in mice. *Cancer Res.* **2009**, *69* (22), 8784–8789.

(15) Song, M.-F.; Li, Y.-S.; Kasai, H.; Kawai, K. Metal nanoparticle-induced micronuclei and oxidative DNA damage in mice. *Journal of Clinical Biochemistry and Nutrition* **2012**, *50* (3), 211–216.

(16) Trenque, I.; Mornet, S.; Duguet, E.; Majimel, J.; Brüll, A.; Teinz, K.; Kemnitz, E.; Gaudon, M. Encapsulation of ZnO particles by metal fluorides: Towards an application as transparent insulating coatings for windows. *Opt. Mater. (Amst).* **2013**, *35* (3), 661–667.

(17) a) Newman, M. D.; Stotland, M.; Ellis, J. I. The safety of nanosized particles in titanium dioxide- and zinc oxide-based sunscreens. *J. Am. Acad. Dermatol.* **2009**, *61*, 685–692; b) http://blog.pharmacymix.com/natural-sunscreens-zinc-oxide-or-titanium-dioxide

(18) a) Colmenares, J. C.; Luque, R. Heterogeneous photocatalytic nanomaterials: prospects and challenges in selective transformations of biomass-derived compounds. *Chem. Soc. Rev.* **2014**, *43* (3), 765–778; b) Su, Y.; Straathof, N. J. W.; Hessel, V.; Noel, T. Photochemical transformations accelerated in continuous flow reactors: basic concepts and applications. *Chem. Eur. J.* **2014**, *20*, 10562-10589; d) Noel, T.; Wang, X.; Hessel, V. Accelerating photoredox catalysis in continuous microflow. *Chimica Oggi* **2013**, *31*, 10-14.

(19) Demir, E.; Creus A.; Marcos, R. Genotoxicity and DNA Repair Processes of Zinc Oxide Nanoparticles. *J. Toxicol. Environ. Health* **2014**, *77*, 1292-1303.

(20) Reddy, K. M.; Feris, K.; Bell, J.; Wingett, D. G.; Hanley, C.; Punnoose, A. Selective toxicity of zinc oxide nanoparticles to prokaryotic and eukaryotic systems. *Appl. Phys. Lett.* **2007**, *90* (213902), 213902-1–213902-3.

(21) Jeng, H. A.; Swanson, J. Toxicity of metal oxide nanoparticles in mammalian cells. *J. Environ. Sci. Health. A. Tox. Hazard. Subst. Environ. Eng.* **2006**, *41* (12), 2699–2711.

(22) Collins, P. J.; Kotterman, M. J. J.; Field, J. A.; Dobson, A. D. W. Oxidation of anthracene and benzo[a]pyrene by laccases from Trametes versicolor. *Appl. Environ. Microbiol.* **1996**, *62* (12), 4563–4567.

(23) Premanathan, M.; Karthikeyan, K.; Jeyasubramanian, K.; Manivannan, G. Selective toxicity of ZnO nanoparticles toward Gram-positive bacteria and cancer cells by apoptosis through lipid peroxidation. *Nanomedicine Nanotechnol. Biol. Med.* **2011**, *7* (2), 184–192.

(24) Bae, B. chan; Na, K. Self-quenching polysaccharide-based nanogels of pullulan/folate-photosensitizer conjugates for photodynamic therapy. *Biomaterials* **2010**, *31* (24), 6325–6335.

(25) Guo, H.; Qian, H.; Idris, N. M.; Zhang, Y. Singlet oxygen-induced apoptosis of cancer cells using upconversion fluorescent nanoparticles as a carrier of photosensitizer. *Nanomedicine Nanotechnology, Biol. Med.* **2010**, *6* (3), 486–495.

(26) Pineda, A.; Balu, A. M.; Campelo, J. M.; Romero, A. A.; Carmona, D.; Balas, F.; Santamaria, J.; Luque, R. A dry milling approach for the synthesis of highly active nanoparticles supported on porous materials. *ChemSusChem.* **2011**, *4*, 1561-1564.

(27) Zheng, Y.; Monty, J.; Linhardt, R. J. Polysaccharide-based nanocomposites and their applications. *Carbohydr. Res.* **2014**, *405* (July), 23–32.

(28) Gómez, M.; Esparza, J. L.; Cabré, M.; García, T.; Domingo, J. L. Aluminum exposure through the diet: Metal levels in AβPP transgenic mice, a model for Alzheimer's disease. *Toxicology* **2008**, *249* (2-3), 214–219.

(29) Macías-García, A.; Díaz-Díez, M. A.; Cuerda-Correa, E. M.; Olivares-Marín, M.; Gañan-Gómez, J. Study of the pore size distribution and fractal dimension of HNO3-treated activated carbons. *Appl. Surf. Sci.* **2006**, *252* (17), 5972–5975.

(30) Sekar, A.; Kim, S. H.; Umar, A.; Hahn, Y. B. Catalyst-free synthesis of ZnO nanowires on Si by oxidation of Zn powders. *J. Cryst. Growth* **2005**, *277* (1-4), 471–478.

(31) Wang, X.; Du, Y.; Liu, H. Preparation, characterization and antimicrobial activity of chitosan-Zn complex. *Carbohydr. Polym.* **2004**, *56* (1), 21–26.

(32) Chheda, J. N.; Román-Leshkov, Y.; Dumesic, J. A. Production of 5-hydroxymethylfurfural and furfural by dehydration of biomass-derived mono- and poly-saccharides. *Green Chemistry*. **2007**, *9*, 342-350.

(33) Tani, T.; Mädler, L.; Pratsinis, S. E. Homogeneous ZnO nanoparticles by flame spray pyrolysis. *J. Nanoparticle Res.* **2002**, *4* (4), 337–343.

(34) Patterson, A. L. The diffraction of X-rays by small crystalline particles. *Phys. Rev.* **1939**, *56* (10), 972–977.

(35) Bagus, P. S.; Ilton, E. S.; Nelin, C. J. The interpretation of XPS spectra: Insights into materials properties. *Surface Science Reports*. **2013**, *68*, 273–304.

(36) Lewin, E.; Persson, P. O. Å.; Lattemann, M.; Stüber, M.; Gorgoi, M.; Sandell, a.; Ziebert, C.; Schäfers, F.; Braun, W.; Halbritter, J.; et al. On the origin of a third

spectral component of C1s XPS-spectra for nc-TiC/a-C nanocomposite thin films. *Surf. Coatings Technol.* **2008**, *202* (15), 3563–3570.

(37) Jing, L.; Xu, Z.; Sun, X.; Shang, J.; Cai, W. The surface properties and photocatalytic activities of ZnO ultrafine particles. *Appl. Surf. Sci.* **2001**, *180* (3-4), 308–314.

(38) Kim, J. S.; Marzouk, H. A.; Reucroft, P. J.; Hamrin, C. E. Characterization of high quality c axis oriented ZnO thin films grown by metal organic chemical vapor deposition using zinc acetate as source material. *Thin Solid Films*. **1992**, *217* (1-2), 133–137.

(39) Grunze, M.; Hirschwald, W.; Hofmann, D. Zinc oxide: Surface structure, stability, and mechanisms of surface reactions. *Journal of Crystal Growth*. **1981**, *52*, 241–249.

(40) Yin, H.; Casey, P. S.; McCall, M. J.; Fenech, M. Effects of surface chemistry on cytotoxicity, genotoxicity, and the generation of reactive oxygen species induced by ZnO nanoparticles. *Langmuir* **2010**, *26* (19), 15399–15408.

(41) Valdiglesias, V.; Costa, C.; Kiliç, G.; Costa, S.; Pásaro, E.; Laffon, B.; Teixeira, J. P. Neuronal cytotoxicity and genotoxicity induced by zinc oxide nanoparticles. *Environ. Int.* **2013**, *55*, 92–100.

(42) Hsiao, I.-L.; Huang, Y.-J. Effects of various physicochemical characteristics on the toxicities of ZnO and TiO nanoparticles toward human lung epithelial cells. *Sci. Total Environ.* **2011**, *409* (7), 1219–1228.

(43) Osmond, M. J.; McCall, M. J. Zinc oxide nanoparticles in modern sunscreens: an analysis of potential exposure and hazard. *Nanotoxicology* **2010**, *4* (1), 15–41.

(44) Kao, Y. Y.; Chiung, Y. M.; Chen, Y. C.; Cheng, T. J.; Liu, P. S. Zinc oxide nanoparticles interfere with zinc ion homeostasis to cause cytotoxicity. *Toxicol. Sci.* **2012**, *125* (2), 462–472.

(45) Deng, X.; Luan, Q.; Chen, W.; Wang, Y.; Wu, M.; Zhang, H.; Jiao, Z. Nanosized zinc oxide particles induce neural stem cell apoptosis. *Nanotechnology* **2009**, *20* (11), 115101.

(46) Yang, X.; Liu, X.; Lu, H.; Zhang, X.; Ma, L.; Gao, R.; Zhang, Y. Real-time investigation of acute toxicity of ZnO nanoparticles on Human Lung epithelia with hopping probe ion conductance microscopy. *Chem. Res. Toxicol.* **2012**, *25* (2), 297–304.

(47) Akhtar, M. J.; Ahamed, M.; Kumar, S.; Khan, M. M.; Ahmad, J.; Alrokayan, S. a. Zinc oxide nanoparticles selectively induce apoptosis in human cancer cells through reactive oxygen species. *Int. J. Nanomedicine* **2012**, *7*, 845–857.

(48) Kang, T.; Guan, R.; Chen, X.; Song, Y. In vitro toxicity of different-sized ZnO nanoparticles in Caco-2 cells. *Nanoscale Res.Lett.* **2013**, *8(1)*, 496.

(49) Hsiao, I. L.; Huang, Y. J. Effects of serum on cytotoxicity of nano- and micro-sized ZnO particles. *J. Nanoparticle Res.* **2013**, *15* , 1829.

(50) Altunbek, M.; Çulha, M. Influence of Surface Properties of Zinc Oxide Nanoparticles on their Cytotoxicity. *Colloids Surfaces B Biointerfaces* **2014**, *121*, 106-113.

(51) Herrmann, R.; García-García, F. J.; Reller, A. Rapid degradation of zinc oxide nanoparticles by phosphate ions. *Beilstein J. Nanotechnol.* **2014**, *5*, 2007–2015.

(52) Fukui, H.; Horie, M.; Endoh, S.; Kato, H.; Fujita, K.; Nishio, K.; Komaba, L. K.; Maru, J.; Miyauhi, A.; Nakamura, A.; et al. Association of zinc ion release and

oxidative stress induced by intratracheal instillation of ZnO nanoparticles to rat lung. *Chem. Biol. Interact.* **2012**, *198* (1-3), 29–37.

(53) Song, W.; Zhang, J.; Guo, J.; Zhang, J.; Ding, F.; Li, L.; Sun, Z. Role of the dissolved zinc ion and reactive oxygen species in cytotoxicity of ZnO nanoparticles. *Toxicol. Lett.* **2010**, *199* (3), 389–397.

(54) (1) Fukui, H.; Horie, M.; Endoh, S.; Kato, H.; Fujita, K.; Nishio, K.; Komaba, L. K.; Maru, J.; Miyauhi, A.; Nakamura, A.; et al. Association of zinc ion release and oxidative stress induced by intratracheal instillation of ZnO nanoparticles to rat lung. *Chem. Biol. Interact.* **2012**, *198* (1-3), 29–37.

(55) Valdiglesias, V.; Costa, C.; Kiliç, G.; Costa, S.; Pásaro, E.; Laffon, B.; Teixeira, J. P. Neuronal cytotoxicity and genotoxicity induced by zinc oxide nanoparticles. *Environ. Int.* **2013**, *55*, 92–100.

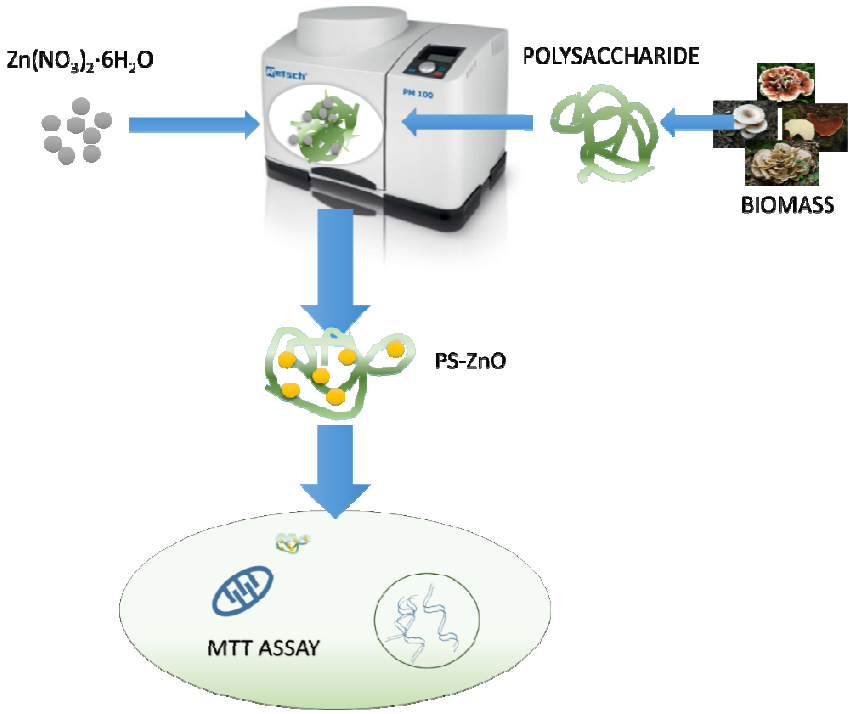

Chunping Xu, Manuel Ojeda, Rick A.D. Arancon, Antonio A. Romero, José Luis Domingo, Mercedes Gómez, Jordi Blanco, Rafael Luque*

Mechanochemically synthesized ZnO nanohybrids using a sustainable dry milling protocol exhibited remarkably low toxicities for *in-vitro* human cell experiments as compared to commercial and literature materials

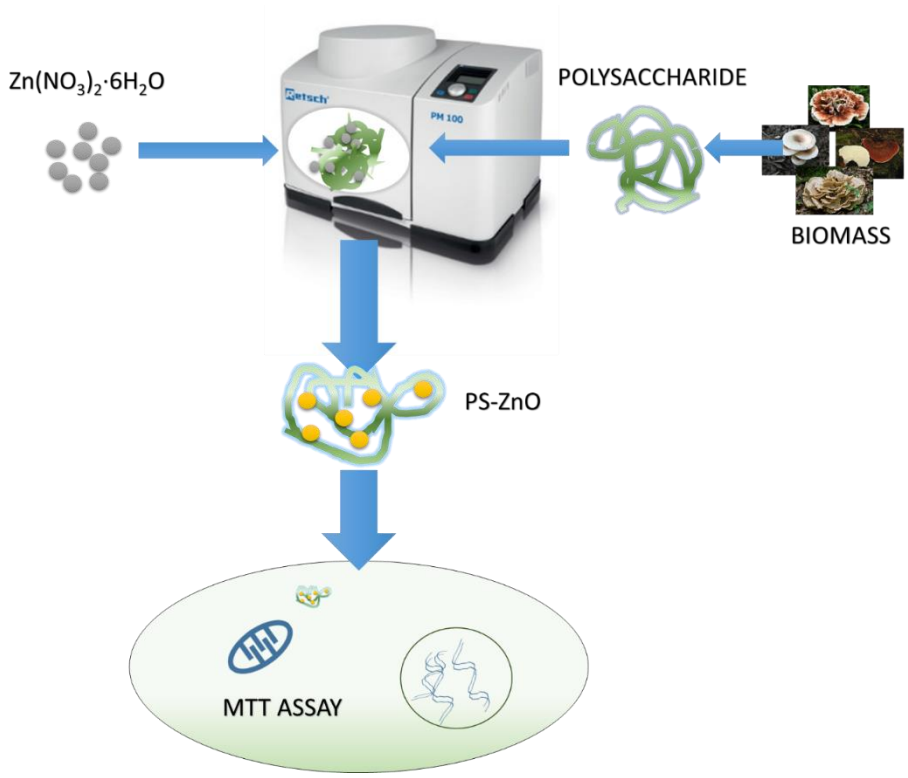

Mechanochemically synthesized ZnO nanohybrids were found to exhibit remarkably low toxicities for *in-vitro* human cell experiments as compared to commercial and literature materials